Distributed predictive secondary control with soft constraints for optimal dispatch in hybrid AC/DC microgrids

Alex Navas-Fonseca, Claudio Burgos-Mellado, Juan S. Gómez, Enrique Espina, Jacqueline Llanos, Doris Sáez, Mark Sumner, and Daniel E. Olivares

***Abstract*—Hybrid AC/DC microgrids (H-MGs) are a prominent solution for integrating distributed generation and modern AC and DC loads. However, controlling these systems is challenging as multiple electrical variables need to be controlled and coordinated. To provide flexibility to the control system, these variables can be regulated to specific values or within secure bands. This paper proposes a set of distributed model predictive control schemes for the secondary control level to control certain variables to specific values and other variables within secure pre-defined bands into H-MGs. Specifically, optimal dispatch of active and reactive power is achieved while frequency and voltages are regulated within secure bands in H-MGs. Dynamic models of AC generators, DC generators and interlinking converters along with their novel multi-objective cost functions are developed in constrained distributed predictive optimisation problems to simultaneously achieve the aforementioned objectives via information sharing. Extensive simulation work validates the performance of this proposal.**

***Index Terms*—Hybrid AC/DC Microgrids, distributed predictive control, secondary controllers, predictive optimal dispatch**

NOMENCLATURE

MG	Microgrid.
H-MG	Hybrid AC/DC Microgrid.
DG	Distributed generator.
ILC	Interlinking converter.
Z_i	AC load.
R_i	DC load.
MPC	Model predictive control.
DMPC	Distributed model predictive control.
LCL	Inductive capacitive inductive filter.
QP	Quadratic programming.
η_i	DG_i's incremental cost.
Ψ_i	DG_i's Reactive marginal cost.
$a_i,\ b_i,\ c_i$	DG_i's constant cost parameters.
$a'_i,\ b'_i$	DG_i's cost parameters for reactive power dispatch.
$S_{i,res},$	DG_i's residual apparent power capacity.
$\mathbb{N}_{ac}$	Set of AC DGs.
$\mathbb{N}_{dc}$	Set of DC DGs.
$\mathbb{N}_{ILC}$	Set of ILCs.
A	Adjacency matrix.
a_{ij}	Communication term between DGs.
τ_{ij}	Communication delay.
$\hat{\tau}_{ij}$	Estimated communication delay.
N_y	Prediction horizon.
N_u	Control horizon.
λ	Weighting parameter in cost functions.
T_{sec}	Predictive controller sample time.
P_i^{dc}	Active power of DC DG_i.
V_i^{dc}	Voltage at the output of the i-th DC-DG.
V_0	Nominal voltage of DC sub-MG.
R_i	Coupling resistor.
G_i	Nominal admittance for DC sub-MG.
$\hat{V}_i^{B,dc}$	Estimated voltage at the coupling point of DC DG_i.
$P_{i,max}$	Maximum active power of DC DG_i.
${}_{\triangle}V^{dc}{}_{s,i}$	Voltage control action variation of DC DG_i.
$V^{dc}{}_{s,i}$	Voltage control action of DC DG_i.
V_0^{dc}	Nominal voltage of AC sub-MG.
$M_{pv,i}$	Active droop slope of DC DG_i.
$V_{aux,i}^{dc}$	Auxiliary optimisation variable for voltage on the DC sub-MG.
$\overline{V}_i^{dc}$	Local AC sub-MG average voltage approximation.
V_{max}^{dc}	Maximum limit for the local average voltage approximation on the DC sub-MG.
V_{min}^{dc}	Minimum limit for the Local average voltage approximation on the DC sub-MG.
$\mathbb{X}_{p,i}^{dc}$	Predicted variables optimisation vector of DC DG_i.
$\mathbb{X}_{\Delta,i}^{dc}$	Predicted control action sequence vector of DC DG_i.
L_i	Coupling inductor.
B_i	Nominal admittance for AC sub-MG.
P_i^{ac}	Active power of AC DG_i.
Q_i	Reactive power of AC DG_i.
$S_{i,max}$	Maximum apparent power of AC DG_i.
V_i^{ac}	Voltage at the output of the i-th AC DG.
ω_i	Angular speed at the output of AC DG_i.
θ_i	Phase angle at the output of AC DG_i.
$\hat{V}_i^{B,ac}$	Estimated voltage at the coupling point of AC DG_i.
$\hat{\omega}_i^B$	Angular frequency at the coupling point of AC DG_i.
$\hat{\theta}_i^B$	Phase angle at the coupling point of AC DG_i.
$\delta\theta_i$	Phase angle deviation of AC DG_i.
${}_{\triangle}\omega_{s,i}$	Frequency control action variation of AC DG_i.

This study was supported by the FONDECYT 1220507 grant, SERC-Chile ANID/FONDAP/15110019, ISCI ANID PIA/PUENTE AFB220003, and from ANID/Doctorado Nacional 2019-21190961 and from Secretaría de Educación Superior, Ciencia, Tecnología e Innovación de Ecuador, SENESCYT/ARSEQ-BEC-005848-2018.

$_{\triangle}V^{ac}{}_{s,i}$	Voltage control action variation of AC DG_i.
$\omega_{s,i}$	Frequency control action.
$V^{ac}{}_{s,i}$	Voltage control action of AC DG_i.
ω_0	Nominal frequency of AC sub-MG.
V_0^{ac}	Nominal voltage of AC sub-MG.
$M_{p\omega,i}$	Active droop slope of AC DG_i.
$M_{qv,i}$	Reactive droop slope of AC DG_i.
$S_{i\,max}$	Maximum apparent power of AC DG_i.
$\omega_{aux,i}$	Auxiliary optimisation variable for frequency on the AC sub-MG.
$V_{aux,i}^{ac}$	Auxiliary optimisation variable for voltage on the AC sub-MG.
$\overline{\omega}_i$	Local average frequency approximation on the AC sub-MG.
$\overline{V}_i^{ac}$	Local AC sub-MG average voltage approximation.
ω_{max}	Maximum limit for the local average frequency approximation on the AC sub-MG.
ω_{min}	Minimum limit for the local average frequency approximation on the AC sub-MG.
V_{max}^{ac}	Maximum limit for the local average voltage approximation on the AC sub-MG.
V_{min}^{ac}	Minimum limit for the Local average voltage approximation on the AC sub-MG.
$\mathbb{X}_{p,i}^{ac}$	Predicted variables optimisation vector of AC DG_i.
$\mathbb{X}_{\Delta,i}^{ac}$	Predicted control action sequence vector of AC DG_i.
$_{\triangle}P^{ILC}{}_h$	Power control action variation of ILC_i.
$\mathbb{X}_{p,h}^{ILC}$	Predicted variables optimisation vector of ILC_i.
$\mathbb{X}_{\Delta,i}^{ILC}$	Predicted control action sequence vector of ILC_i.

I. Introduction

MICROGRIDS (MGs) are driving the integration of distributed generation (DG) units, transforming the traditional centralised power grid. Isolated MGs must autonomously regulate all the electrical variables and achieve an efficient operation of their generation units. Depending on their grid configuration, MGs can be classified as AC MGs, DC MGs, and Hybrid AC/DC MGs (H-MGs) [1]. The latter improves the system efficiency by reducing conversion stages, conversion losses, and operation cost [1]–[3]. H-MGs are typically composed of an AC sub-MG, a DC sub-MG, and interlinking converters (ILCs), where the ILCs transfer power bidirectionally between the AC sub-MG and the DC sub-MG, as shown in Fig. 1.

H-MGs, and MGs in general, inherit the three-level hierarchical control structure of traditional power systems. The primary control level compensates for load changes by means of voltage and frequency deviations, preserving MG's stability (droop control), while the main task of the secondary level is restoring the aforementioned variables to nominal values [4]. On the other hand, the tertiary level is typically in charge of the optimal dispatch of DGs, considering their generation costs, and coordination of neighbouring MGs [4]–[6]. However, latest research for DC MGs [7], [8], AC MGs [9]–[13] and H-MGs [14], [15] has demonstrated that due to the susceptibility of isolated MGs to fast changes in generation and demand, the optimal dispatch should be performed in a time-scale consistent with that of the secondary control level for it to be adequate. Moreover, usually, only the optimal dispatch of active power is considered, neglecting the optimal dispatch of reactive power. The latter might result in increased operating costs and deviations in the dispatches from the optimal solution. This is because the active power capacity is restricted by using part of the apparent power capacity to generate reactive power. Additionally, a dispatch of reactive power could be beneficial to operate the MG under both imbalance [16] and low-voltage ride-through [17] conditions.

Focusing on the secondary level, there are three types of control architectures: centralised, decentralised, and distributed [18]. Centralised controllers require communication among all the DGs and ILCs (which is impractical for large systems), presenting a high computational burden and a single-point-of-failure [1], [18], [19]. On the other hand, decentralised controllers only handle local information, and allow limited coordination between DGs and ILCs [1], [6]. Conversely, distributed schemes present a more compelling solution, achieving global objectives via coordination of DGs by considering only information from communicating neighbouring DGs [1], [6], [18]–[20], thus facilitating a plug-and-play operation and the MG's scalability. Moreover, robustness against communication failures is provided.

The vast majority of distributed control proposals at the secondary level are based on proportional-integral (PI) controllers, and only address some of the previously described problems, i.e., power sharing of active and reactive power in a faster time-scale [3], [7], [8], [10], [11], [21]. Furthermore, most approaches in the literature assume fixed operational set-points for voltage and frequency, and do not take advantage of the flexibility associated with the secure operational bands defined in IEEE standard 1547-2018 [22]. This standard suggests that AC DGs can operate normally as long as the frequency is within a band of 2% of its nominal value and the voltage is within a band of 0.88 to 1.1 p.u. of its nominal value. Similarly, [23] states that the same standards for AC systems can be used for DC systems without reformulation, nevertheless, the maximum allowable limits may be open to further discussion. For instance, the IEEE 1709-2018 [24] recommends that the voltage limits for DC systems should be within 0.9 to 1.1 p.u.. Note that these limits are quite similar to the recommend in [22]. Also, existing control approaches for driving H-MGs, are designed independently for either AC sub-MGs [5], [10]–[13], [21], [25] or DC sub-MGs [7], [8], without accounting for the particular aspects of hybrid MGs. In particular, the optimal dispatch of AC sub-MGs with frequency restoration is considered in [10]–[13]; however, these works do not account for voltage regulation and reactive power management. Noteworthy, all the aforementioned works assume that frequency and voltages must be set to fixed nominal values, giving up flexibility in the microgrid control system. Also, as most of these work are based on PI controller, it is difficult to achieve multiple objectives and cope with operation constraints [26], [27].

Due to the limitations of PI controllers for H-MG applications [28], distributed model predictive control (DMPC) has attracted the attention of the scientific community related to MGs [5], [12]. DMPC is based on a model of a local system and the prediction of its behaviour over a prediction horizon. Each local controller computes an optimal control sequence based on its local measurements, and information received from neighbouring controllers [29]. DMPC presents a higher computational burden than PI-based approaches, but its computational burden is lower than centralised MPC approaches. Moreover, it does not increase when more DGs are added to the MG. The information is updated, and the process is repeated at each sample time (rolling horizon). The rolling horizon property compensates for communication delays [9], [27], [28]. DMPC can model complex multivariable systems, control multiple objectives, and handle hard and soft constraints [26]–[28]. For H-MGs operation, DMPC can handle DGs and ILCs power rating limits (hard constraint), and regulate variables such as frequency and voltages within secure bands (soft constraints) instead of specific values, making the H-MG operation more flexible [25]. For these reasons, DMPC is one of the most prominent solutions for managing H-MGs as a single entity. The work of [12] proposed a DMPC for frequency regulation and active power dispatch in isolated MGs. However, this work needs knowledge of the load connected. Similarly, [5] proposes a DMPC for grid-connected MGs which includes controllers for DGs, storage devices and loads. Although these works proposed adequate solutions for AC MGs, neither dispatch of reactive power was considered nor its operation in a H-MG.

Focusing on the ILC's power transfer control, there are two main approaches for controlling the power transferred through the ILC. The first one is based on the difference of the normalised deviations of the primary variables with respect to minimum and maximum allowed values, i.e., frequency of the AC sub-MG and voltage of the DC sub-MG [30], [31], which is fed to a PI controller. However, this approach losses accuracy when these variables are regulated by a secondary control. The second approach includes the power management task at the secondary control level [2], [3], [14], [15], [32], [33], where diverse objectives can be defined, such as power sharing [2], [3], [32] and optimal dispatch [14], [15]. Nevertheless, most of the existing approaches consider that the H-MG is composed of three independent systems [2], [14], [15], [30]–[33] (AC sub-MG, DC sub-MG, and ILCs) and neglect the dynamic interactions between them, which can degrade the controllers dynamic response. For instance, in [2], active and reactive powers are shared proportionally to the DGs' power ratings and frequency and voltage are restored to nominal values. Moreover, only the controllers of the ILCs regulate the power transference through the ILCs, as communication between AC DGs and DC DGs is not possible. Furthermore, most of these formulations neither consider limits for the operation of DGs and ILCs, nor reactive power dispatch. A comparison of the latest reported approaches for H-MGs and their objectives is presented in Table I.

Based on the literature review, we identified that it is important to manage properly active and reactive power in a H-MG. Moreover, the physical capacities of DGs and ILCs should be considered by the control system. On the other hand, important variables such as frequency and voltages need to be regulated considering the recommendations of the IEEE 1547-2018 standard to provide flexibility to the H-MGs' operation [22]. Moreover, all these objectives can be fulfilled simultaneously via an advance distributed control strategy such as DMPC to ease the computational burden and the scalability of a H-MG while improving its operation.

Motivated by the gaps discussed above, this paper proposes a DMPC scheme for H-MGs with the following characteristics. First, active power dispatch in AC DGs, DC DGs, and ILCs is determined based on an economic criterion [11], [32]. This is done in a distributed fashion using the incremental cost (IC) consensus principle [10], [11]. In the same fashion, AC DGs supply reactive power based on their residual VA capacity and its generation cost [34], [35]. Furthermore, frequency and voltages are regulated within bands based on the recommendation of IEEE standard 1547-2018 [22], instead of restored to nominal values. The proposed DMPC considers the existence of multiple ILCs, which are operated to simultaneously achieve the cost-effective optimal operation of the H-MG, and avoid overloading of ILCs and circulating currents. Moreover, to predict the behaviour of ILCs and DGs, the dynamic models that rule each of them are included as equality constraints in their respective optimisation problems.Table I summarises the advantages of the proposed DMPC approach for H-MGs compared with the latest works published in this research area.

The proposed DMPC is multi-objective, as it tackles simultaneously consensus objectives to specific values, i.e., optimal dispatch of active power and reactive power, and flexible objectives, i.e., regulation of frequency and voltage within secure bands (based on the IEEE std 1547-2018 [22]). To the best of the authors' knowledge, this is the first paper that considers all these objectives within the formulation of a DMPC scheme. The contributions of this paper are detailed as follows:

i) A cooperative DMPC scheme that considers the interaction among ILCs, AC DGs and DC DGs in isolated H-MGs is proposed. This DMPC scheme controls the H-MG as a single entity instead of three separated systems, providing redundancy to communications and improving the controller's dynamic response. This is the first work that proposes a DMPC that considers the H-MG as a single entity by modelling the interaction between AC DGs, DC DGs and ILCs. Conversely, previous works [14], [15], [31]–[33] model the H-MG as three separated systems.

ii) To the best of the authors' knowledge, this is the first work that considers a DMPC scheme for H-MGs that is flexible enough to manage frequency and voltages within safe bands rather than rigid set points. Moreover, the optimal dispatch of active and reactive power is achieved at the same time. Novel cost functions are proposed to control ILCs, DC DGs, and AC DGs. To predict the behaviour of ILCs and DGs, the dynamic models that rule each of them are included as equality constraints in their respective optimisation problems. Physical saturation (overloading) of AC DGs, DC DGs, and ILCs is avoided by including maximum power rating

TABLE I
COMPARISON OF THE LATEST APPROACHES REPORTED FOR H-MGS

Ref.	Operation principle	CM	FR	VR	PL	RD	MILC
[2]	DMPC	✗	✓	✓	✓	✗	✓
[3]	Consensus-PI	✗	✓	✓	✗	✗	✓
[14]	Consensus-PI	✓	✓	✓	✗	✗	✗
[15]	Consensus-PI	✓	✓	✓	✗	✗	✗
[31]	Consensus-PI	✗	✓	✓	✗	✗	✗
[32]	Consensus-PI	✗	✗	✗	✗	✗	✓
[33]	Consensus-PI	✗	✓	✓	✗	✗	✗
Proposed strategy	DMPC	✓	✓	✓	✓	✓	✓

CM: Cost minimisation **FR:** Frequency regulation **RD:** Reactive power dispatch
PL: Power limits **VR:** Voltaje regulation **MILC:** Multiple ILCs

constraints in the DMPC formulations.

iii) Extensive simulation studies validate that the proposed DMPC has good performance under load change and communication delays scenarios. Also, this paper shows that implementing the optimal dispatch at the secondary level reduces the operation costs of a H-MG considerably.Finally, Table I shows the advantages of this proposal compared to previous reported works.

The remainder of this paper is organised as follows. Section II states the framework of the hybrid MG configuration used. Section III-C and Section III-B present the DMPC formulation for the AC sub-MG and the DC sub-MG, respectively. Section III-A explains in detail the DMPC controller for the ILC. The H-MG setup and the results are presented in Section IV. Finally, the conclusions and future research are discussed in Section V.

II. BACKGROUND

A. Communication structure

Although AC DGs, DC DGs and ILCs have different operating principles, they can interact among them at the secondary control level to achieve global objectives in a distributed control structure [3], as shown in Fig. 1. In this way, information can be shared globally to achieve cooperative control objectives via a fully-meshed communication network. Consider a H-MG composed of a set of $\mathbb{N}$ nodes (DGs or ILCs), where $\mathbb{N} = \mathbb{N}_{ac} \cup \mathbb{N}_{dc} \cup \mathbb{N}_{ILC}$. The subsets of AC DGs, DC DGs, and ILCs are represented for $\mathbb{N}_{ac} = \{1, ..., N_{ac}\}$, $\mathbb{N}_{dc} = \{1, ..., N_{dc}\}$, and $\mathbb{N}_{ILC} = \{1, ..., N_{ILC}\}$, respectively. Each node (DG or ILC) includes a model of the full-duplex communication network. This model considers both latency and connectivity issues. Latency (represented in sampling periods) is characterised as the end to end communication delay (τ_{ij}), i.e., total time for a data packet to be transmitted from source to destination. On the other hand, connectivity represents the information flow among nodes at time instant k and is stated by the $\mathbb{N} \times \mathbb{N}$ non-negative adjacency matrix $\boldsymbol{A}$. The entries a_{ij} of the adjacency matrix $\boldsymbol{A}$ are 1 if there is communication between node *j* and node *i* at k or 0 otherwise, where $k = nT_{sec}, n \in \mathbb{Z}^+$, and T_{sec} is the DMPC sample time.

As a full-duplex communication network is used, the associated communication graph is *undirected*. Thus, $\tau_{ij} = \tau_{ji}$ and a_{ij}=a_{ji} [20]. We consider that the *undirected* graph in this work is *connected*, which implies that there must be at least one communication path between any two nodes (i.e., there is a spanning tree). Moreover, The MG's topology can vary as long as there is at least one communication path among all its nodes.

There are limitations regarding communications to be considered when the proposed scheme is implemented in a real MG. Note that the proposed scheme does not require information about the MG topology for solving the optimisation problems, instead, optimisation variables (described in Section III) are computed by each DG and ILC in the previous sampling period and shared through the communication network. This network has a meshed topology, which means the information flows between terminal points (DGs or ILCs) avoiding bottleneck issues, which are typical in centralised (star) topologies [36]. In this sense, distributed communication protocols such as DNP3 [37] and IEC61850 [38] are required for MG implementations. On the other hand, when the MG scales up, the total information volume flowing through the network increases as well. However, the proposed approach just requires one communication path between DGs or ILCs in the H-MG to satisfy the graph connectivity requirement and achieve the global objectives in a distributed manner [20]. This capability is important for remote area applications, where communication network topology is limited by local geography or reduced budget investment.

B. Active power optimal dispatch problem

The traditional centralised active power optimal dispatch of a H-MG can be expressed as the optimisation problem in (1). The objective function minimises a quadratic cost function subject to the power balance constraint with $\mathbf{P} = \{P_i : i \in \mathbb{N}_{ac} \cup \mathbb{N}_{dc}\}$. P_i is the active power contribution of DG i. The aggregated active power load on AC and DC sub-MGs are P_D^{ac} and P_D^{dc}, respectively. The quadratic cost function for DG_i is expressed in (2), where a_i, b_i and c_i are the cost coefficients of DG_i, defined in Table III.

$$\underset{\mathbf{P}}{\text{minimise}} \quad \sum_{i \in \mathbb{N}_{ac} \cup \mathbb{N}_{dc}} \mathbb{C}_i(P_i) \tag{1a}$$

$$\text{subject to} \quad \sum_{i \in \mathbb{N}_{ac} \cup \mathbb{N}_{dc}} P_i = P_D^{ac} + P_D^{dc} \tag{1b}$$

$$\mathbb{C}_i(P_i) = a_i P_i^2 + b_i P_i + c_i \tag{2}$$

However, as it is demonstrated in [7], [8], [11], this optimisation problem is susceptible to single-point-of-failure and high computational burden if it is solved using a centralised approach. For these reasons, a distributed controller is a most reliable and secure solution. The optimisation problem of (1) can be expressed in a distributed way through the incremental

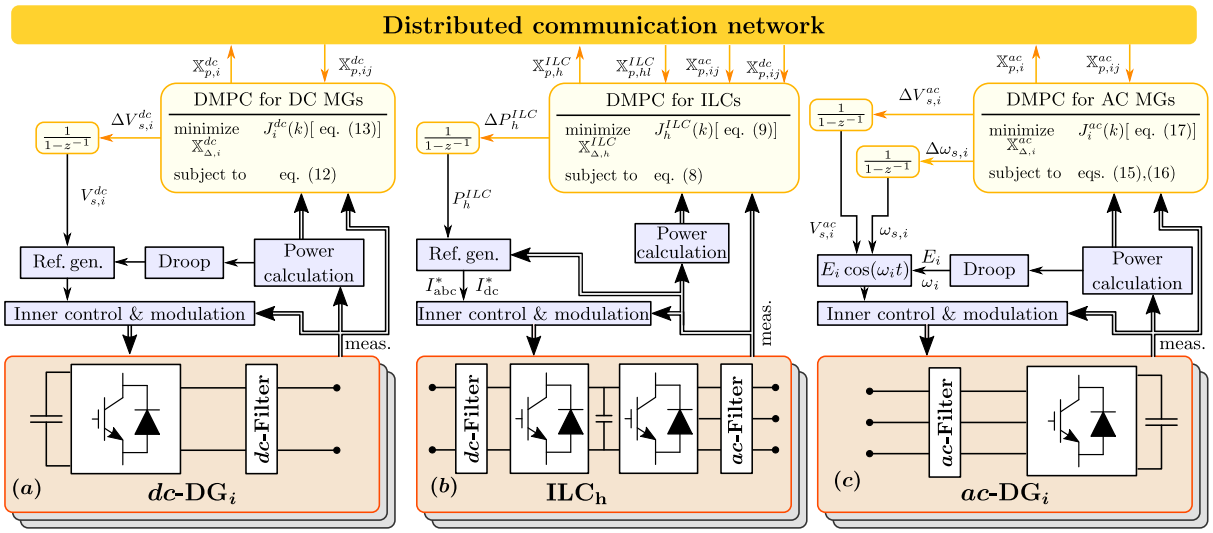

Fig. 1. Proposed DMPC scheme for the control of isolated hybrid AC/DC MGs.

cost criterion [9]–[11]. The Lagrangian function of (1) can be expressed as follows.

$$\mathbb{L}\left(P_i,\eta\right)=\sum_{i\in N_{ac}\cup N_{dc}}\mathbb{C}_i\left(P_i\right)+\eta\left(P_D^{ac}+P_D^{dc}-\sum_{i\in N_{ac}\cup N_{dc}}P_i\right) \tag{3}$$

$$\frac{\partial\mathbb{L}\left(P_i,\eta\right)}{\partial P_i}=0\quad\Longleftrightarrow\quad\eta=\frac{\partial\mathbb{C}_i\left(P_i\right)}{\partial P_i},\quad i\in\mathbb{N}_{ac}\cup\mathbb{N}_{dc} \tag{4}$$

From the stationary condition (4), the incremental cost (IC) or Lagrange operator η can be obtained. To accomplish the active power optimal dispatch of the H-MG, all DGs must achieve the same IC, i.e., $\eta=\eta_i=\eta_j$ where $i,j\in\mathbb{N}_{ac}\cup\mathbb{N}_{dc}$.

C. Reactive power optimal dispatch problem

As the total generation costs of AC-DGs are associated with the active and reactive power supplied, it is necessary to co-optimise the production of reactive power in the AC sub-MG [39]. For this purpose, similarly to the IC principle described in Section II-B, the reactive marginal cost (RMC) in (5) is proposed to minimise the production of reactive power in a distributed fashion [34], [35], where Q_i is the reactive power of AC-DG i and $S_{i,res}$ is the residual apparent power capacity of AC-DG i as reason of its rated capacity, i.e., $S_{i,res}=(S_{i,max}-S_i)/S_{i,max}$.

$$\Psi_i=2a_i'\,S_{i,res}\,Q_i+b_i'\quad i\in\mathbb{N}_{ac} \tag{5}$$

The cost coefficients $a_i'=a_i\,sin^2(\phi)$ and $b_i'=b_i\,sin(\phi)$ depend on the active power cost parameters (defined in Table III) and the power factor's angle ϕ. To accomplish the reactive power optimal dispatch of the AC sub-MG, all AC DGs must achieve the same RMC, i.e., $\Psi=\Psi_i=\Psi_j$ where $i,j\in\mathbb{N}_{ac}$. Based on the IC and RMC principles, a novel cooperative DMPC strategy is proposed. This strategy minimises the operational costs of both active and reactive power while the voltages on both sub-MGs and the frequency (on the AC sub-MG) are regulated within bands.

III. DMPC FORMULATION FOR H-MGS

The following explanations and mathematical analysis are done for ILC_h, DC DG_i, and AC DG_i, as the analysis is analogous for the rest of the ILCs and DGs. For ILCs and DC DGs, the phenomenological models used in the DMPCs are presented first, and later their predictive version is derived. In contrast, only the prediction models are presented for the AC DGs. However, the interested reader is encouraged to consult the previous work of some of this paper's authors [40] for a detailed explanation of the phenomenological models for AC DGs. Finally, the incremental operator (6) is used to express the predictive controllers in function of the control variations and it will be explained in the controllers' formulation.

$$\Delta f(k)=f(k)-f(k-1) \tag{6}$$

A. DMPC for interlinking converters (ILCs)

The DMPC for ILCs has two control objectives. The first objective is to guarantee the economic operation of the H-MG by transferring power from the cheapest sub-MG to the most expensive sub-MG. The second objective is to ensure that the power transferred through each ILC is proportional to its power rating to avoid overloading the ILCs. As stated before, the ILC transfers active power bidirectionally between the sub-MGs. In this way, to achieve active power optimal dispatch in a H-MG, the ILC should equalise the ICs of both sub-MGs, i.e., the condition $\eta_i^{ac}=\eta_j^{dc}=\eta$ must hold, where $i\in\mathbb{N}_{ac}\wedge j\in\mathbb{N}_{dc}$ and η is the optimal IC value. The control diagram of ILC_h with $h\in\mathbb{N}_{ILC}$ is depicted in Fig. 2. Two control levels are distinguished. As a back-to-back configuration is used for each ILC, the primary level comprises a current controller on

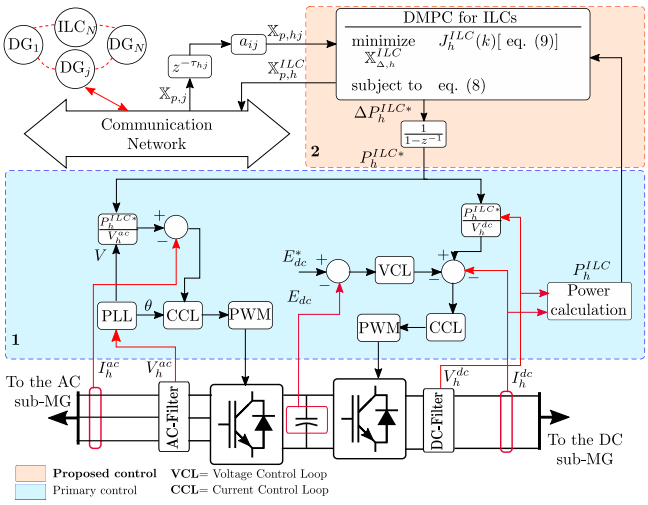

Fig. 2. Control diagram of DMPC_i for ILCs.

both AC and DC sides. In contrast, the proposed DMPC is presented at the secondary level.

The DMPC receives as inputs the local active power measurement (P_h^{ILC}) and the active power predictions of communicated *ac* DGs, *dc* DGs, and ILCs. The controller has two outputs, which are the active power variation (vector ${}_{\triangle}P_h^{ILC}$) and the results of the local optimisation problem $\mathbb{X}_{p,h}^{ILC}$ (vector of predicted values), both defined later in this section. Furthermore, due to information sharing, the ILCs can be connected to any electrical node in the MG. Considering that the losses in ILC_h are negligible and power is being transferred from the DC sub-MG to the AC sub-MG, the power contributions, model (7a) can compute the current active power contribution of the i-th AC DG ($P_i^{ac}(k)$) as its previous (measured) active power ($P_i^{ac}(k-1)$) added to the power supplied (measured) by the ILC ($P_(h,i)^{ILC}(k-1)$). Similarly, as power is being supplied from the DC sub-MG to the AC sub-MG, model (7b) can compute the current active power contribution of the j-th DC DG ($P_j^{dc}(k)$).

$$P_i^{ac}(k) = P_i^{ac}(k-1) + P_{h,i}^{ILC}(k-1) \quad \forall\ i \in \mathbb{N}_{ac} \tag{7a}$$

$$P_j^{dc}(k) = P_j^{dc}(k-1) - P_{h,j}^{ILC}(k-1) \quad \forall\ j \in \mathbb{N}_{dc} \tag{7b}$$

The set of prediction models included in the DMPC of ILC_h are presented in (8). The previous discrete time models are generalised for $k+m$ steps ahead in (8a) and (8b), where $m \in \mathbb{Z}^+$. Additionally, the incremental operator (6) is applied to derive the power contributions as a function of their variation (${}_{\triangle}P_{h,i}^{ILC}$). To obtain the active power reference variation (${}_{\triangle}P_h^{ILC}$) for ILC_h, the power contributions from each DG are added in (8c). A discrete time integrator is used to get the power reference for ILC_h, ensuring zero error in steady-state, as shown in Fig. 2. Note that $P_h^{ILC} > 0$ indicates that power is flowing from the DC sub-MG to the AC sub-MG. The IC models for AC DGs and DC DGs are presented in (8d) and (8e), respectively. Finally, the ILC's maximum active power rating model is included in (8f) to guarantee that the power reference is within the physical capacity of ILC_h.

$$\begin{aligned} P_i^{ac}(k+m) =& 2P_i^{ac}(k+m-1) - P_i^{ac}(k+m-2) \\ &+ {}_{\triangle}P_{h,i}^{ILC}(k+m-1) \quad \forall\ i \in \mathbb{N}_{ac} \end{aligned} \tag{8a}$$

$$\begin{aligned} P_j^{dc}(k+m) =& 2P_j^{dc}(k+m-1) - P_j^{dc}(k+m-2) \\ &- {}_{\triangle}P_{h,j}^{ILC}(k+m-1) \quad \forall\ j \in \mathbb{N}_{dc} \end{aligned} \tag{8b}$$

$$\begin{aligned} {}_{\triangle}P_h^{ILC}(k+m-1) = \sum_{i\in\mathbb{N}_{ac}} a_{ih}(k) {}_{\triangle}P_{h,i}^{ILC}(k+m-1) = \\ \sum_{j\in\mathbb{N}_{dc}} a_{jh}(k) {}_{\triangle}P_{h,j}^{ILC}(k+m-1) \end{aligned} \tag{8c}$$

$$\eta_i^{ac}(k+m) = 2a_i P_i^{ac}(k+m) + b_i \quad \forall\ i \in \mathbb{N}_{ac} \tag{8d}$$

$$\eta_j^{dc}(k+m) = 2a_j P_j^{dc}(k+m) + b_j \quad \forall\ j \in \mathbb{N}_{dc} \tag{8e}$$

$$P_{h,min}^{ILC} \le P_h^{ILC}(k+m-1) \le P_{h,max}^{ILC} \tag{8f}$$

The cost function of the DMPC for ILC_h is described in (9) where N_y and N_u are the prediction and the control horizons, respectively. The first term penalises the variation of the control action sequence to minimise the control effort and improve the controller's transient behaviour. The second term equalises the ICs of the sub-MGs by transferring power from the cheapest side to the most expensive side. When all DGs achieve a consensus in the IC, the optimal dispatch equilibrium is reached. This objective is strengthened in each DG controller, as explained in Section III-B and Section III-C. The third term ensures that, when there are multiple ILCs, the power transferred per each ILC is proportional to its power rating with $l \in \mathbb{N}_{ILC}$. Thus, avoiding overloading the ILCs. The terms λ_{1h} to λ_{3h} are positive tuning parameters. Note that the cooperative objectives (optimal dispatch of DGs and power sharing of ILCs) are updated only with the predicted information of communicated neighbouring *agents*, represented by the terms $a_{hi}(k)$, $a_{hj}(k)$ and $a_{hl}(k)$, and the estimated delays $\hat{\tau}_{hi}$, $\hat{\tau}_{hj}$ and $\hat{\tau}_{hl}$.

$$\begin{aligned} J_h^{ILC}(k) =& \sum_{k=1}^{N_u} \lambda_{1h} ({}_{\triangle}P_h^{ILC}(k+m-1))^2 \\ &+ \sum_{i\in\mathbb{N}_{ac}} \sum_{j\in\mathbb{N}_{dc}} \sum_{k=1}^{N_y} \lambda_{2h} a_{hi}(k) a_{hj}(k) \left(\eta_i^{ac}(k+m-\hat{\tau}_{hi}) - \eta_j^{dc}(k+m-\hat{\tau}_{hj})\right)^2 \\ &+ \sum_{l\in\mathbb{N}_{ILC}} \sum_{k=1}^{N_y} \lambda_{3h} a_{hl}(k) \left(\frac{P_h^{ILC}(k+m)}{P_{h\,\max}^{ILC}} - \frac{P_l^{ILC}(k+m-\hat{\tau}_{hl})}{P_{l\,\max}^{ILC}} \right)^2 \end{aligned} \tag{9}$$

The proposed DMPC comprises a quadratic cost function, linear equality constraints and linear inequality constraints; thus, it is convex and can be synthesised in a canonical quadratic programming (QP) formulation. The optimisation vector of the QP problem comprises the predicted variables $\mathbb{X}_{p,h}^{ILC}$ and the control decisions $\mathbb{X}_{\Delta,h}^{ILC}$ presented in (10a) and

(10b), respectively. The former is sent to the communication network and the first control decision of the latter, $_{\triangle}P_h^{ILC}(k)$, is applied to ILC_h, after passing through an integrator (see Fig. 2). At each sample time the optimisation problem is computed with updated measures (rolling horizon) [29].

$$\mathbb{X}_{p,h}^{ILC} = \{P_i^{ac}(k+m), P_j^{dc}(k+m), P_h^{ILC}(k+m), \eta_i^{ac}(k+m), \eta_j^{dc}(k+m)\}_{k=1}^{N_y} \tag{10a}$$

$$\mathbb{X}_{\Delta,h}^{ILC} = \{_{\triangle}P_h^{ILC}(k+m-1)\}_{k=1}^{N_u} \tag{10b}$$

B. DMPC for the DC sub-microgrid

The DMPC for DC DGs has three control objectives. The first and second objectives are to guarantee the economic dispatch of the H-MG via the incremental cost consensus with DC DGs and AC DGs. The third objective is to regulate the average voltage on the DC sub-MG within secure bands to provide flexibility to the H-MG. The control scheme for the DC DG_i is depicted in Fig. 3, where the primary control (see at the bottom) is based on $P-V$ droop control [3], [7] and the proposed DMPC for secondary level is presented at the top. The local measurements/estimates $(P_i^{dc}(k), V_i^{dc}(k), \hat{V}_i^{dc,B}(k))$ and the results of the optimisation problems of communicated neighbouring units are the inputs of the DMPC. The controller has two outputs, which are the voltage control action variation (vector $_{\triangle}V_{s,i}^{dc}$) and the results of the local optimisation problem $\mathbb{X}_{p,i}^{dc}$ (vector of predicted values), both defined later in this section. This controller includes the $P-V$ droop control and the power transfer models, as shown in (11). V_i^{dc} is the output voltage of DC DG_i as is computed in (11a), P_i^{dc} is the active power transferred to the MG, computed by (11b), V_0^{dc} is the nominal voltage of the DC sub-MG, $M_{pv,i}$ is the droop slope, and $V_{s,i}^{dc}$ is the secondary control action. Equation (11b) determines the power contribution of DG_i to the MG. Note that a complete electrical model of the MG is not needed by using (11b). Moreover, (11b) only uses local measurements and the voltage estimation $\hat{V}_i^{dc,B}$ after the coupling resistor R_i (with $G_i = 1/R_i$), which is computed through the Ohm's law.

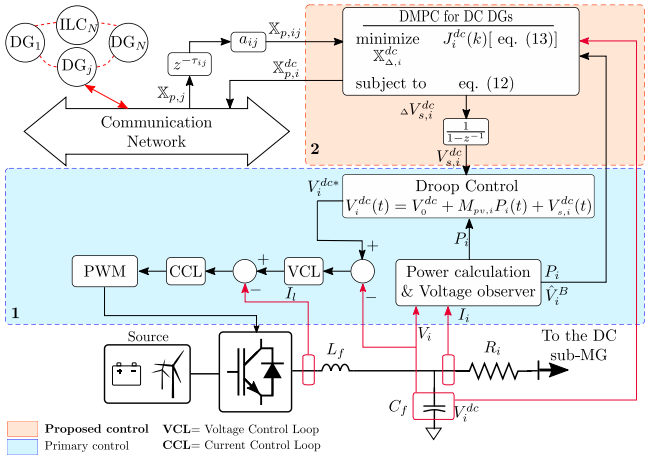

Fig. 3. Control diagram of DMPC$_i$ for DC DGs.

$$V_i^{dc}(t) = V_0^{dc} + M_{pv,i} P_i^{dc}(t) + V_{s,i}^{dc}(t) \tag{11a}$$

$$P_i^{dc}(t) = G_i V_i^{dc}(t)(V_i^{dc}(t) - \hat{V}_i^{dc,B}(t)) \tag{11b}$$

The set of equations in (12) present the discrete time models included as equality and inequality constraints in the DMPC formulation for DC DGs. Models (12a) and (12b) are the discretised versions of (11) via the forward Euler method, where in the former, the incremental operator (6) was applied and in the latter a Taylor expansion around the measured/estimated point$\{V_i(k),\ \hat{V}_i^{dc,B}(k), P_i^{dc}(k)\}$ is used. Model (12c) represents the IC of the DC DGi, while a local average DC voltage approximation ($\overline{V}_i^{dc}$) is computed in (12d). Note that $\overline{V}_i^{dc}$ also depends on the communication terms $a_{ij}(k)$ and the estimated delay $(\hat{\tau}_{ij})$. The active power contribution is limited within the DG's power rating in (12e). Finally, the soft constraint (12f) works in conjunction with the cost function (see third term of (13)) to regulate the average DC voltage in a predefined band within the recommendation of IEEE standard 1547-2018 [22] and avoid unfeasible solutions [29], where $V_{aux,i}^{dc}$ is an auxiliary variable that acts as a slack variable.

$$V_i^{dc}(k+m) = M_{pv,i}[P_i^{dc}(k+m) - P_i^{dc}(k+m-1)] + V_i^{dc}(k+m-1) + {}_{\triangle}V_{s,i}^{dc}(k+m-1) \tag{12a}$$

$$P_i^{dc}(k+m) = [V_i^{dc}(k+m) - V_i^{dc}(k)] G_i [2V_i^{dc}(k) - \hat{V}_i^{dc,B}(k)] + P_i^{dc}(k) \tag{12b}$$

$$\eta_i^{dc}(k+m) = 2a_i P_i^{dc}(k+m) + b_i \tag{12c}$$

$$\overline{V}_i^{dc}(k+m) = \frac{V_i^{dc}(k+m) + \sum_{j \in \mathbb{N}_{dc}} a_{ij}(k) V_j^{dc}(k+m-\hat{\tau}_{ij})}{1 + \sum_{j \in \mathbb{N}_{dc}} a_{ij}(k)} \tag{12d}$$

$$P_{i,\min}^{dc} \leq P_i^{dc}(k+m) \leq P_{i,\max}^{dc} \tag{12e}$$

$$\overline{V}_{min}^{dc} \leq \overline{V}_i^{dc}(k+m) + V_{aux,i}^{dc}(k+m) \leq \overline{V}_{max}^{dc} \tag{12f}$$

The cost function (13) is composed of four quadratic terms. The first term achieves the consensus over the ICs within the DC DGs, while the second term performs the consensus for the ICs of the AC DGs. The latter objective only works when the ILCs are enabled; the controller verifies the ILCs status (1: ON, 0:OFF) at each sample time. The third term achieves the regulation of the average DC voltage within a band by penalising the auxiliary variable $V_{aux,i}^{dc}$. This term temporally

relaxes the average DC voltage regulation constraint (12f), allowing the average DC voltage to take transient values outside its predefined band when the MG is disturbed. The last term penalises the control effort to achieve all the previous objectives with good transitory behaviour. The terms λ_{1i} to λ_{4i} are positive tuning parameters. Note that the cooperative objectives (IC consensus with DC DGs and with AC DGs) are updated only with the predicted information of communicated neighbouring DGs, represented by the terms $a_{ij}(k)$, and the estimated delays $\hat{\tau}_{ij}$.

$$\begin{aligned} J_i^{dc}(k) = &\sum_{j\in\mathbb{N}_{dc}}\sum_{m=1}^{N_y}\lambda_{1i}a_{ij}(k)\left(\eta_i^{dc}(k+m)-\eta_j^{dc}(k+m-\hat{\tau}_{ij})\right)^2 \\ &+\sum_{j\in\mathbb{N}_{ac}}\sum_{m=1}^{N_y}\lambda_{2i}a_{ij}(k)\left(\eta_i^{dc}(k+m)-\eta_j^{ac}(k+m-\hat{\tau}_{ij})\right)^2 \\ &+\sum_{m=1}^{N_y}\left[\lambda_{3i}(V_{aux,i}^{dc}(k+m))^2\right]+\sum_{k=1}^{N_u}\lambda_{4i}(\triangle V_{s,i}^{dc}(k+m-1))^2 \end{aligned} \tag{13}$$

The proposed DMPC is synthesised in a QP formulation. The optimisation vector of the QP problem comprises the predicted variables $\mathbb{X}_{p,i}^{dc}$ and the control decisions $\mathbb{X}_{\Delta,i}^{dc}$ presented in (14a) and (14b), respectively. The former is sent to the communication network and the first control decisions of the latter, $\triangle V_{s,i}^{dc}(k)$, is applied to the DG, after passing through an integrator (see Fig. 3). At each sample time the optimisation problem is computed with updated measures (rolling horizon) [29].

$$\mathbb{X}_{p,i}^{dc} = \{\overline{V}_i^{dc}(k+m), V_i^{dc}(k+m), P_i^{dc}(k+m), \eta_i^{dc}(k+m)\}_{k=1}^{N_y} \tag{14a}$$

$$\mathbb{X}_{\Delta,i}^{dc} = \{\triangle V_{s,i}^{dc}(k+m-1)\}_{k=1}^{N_u} \tag{14b}$$

C. DMPC for the AC sub-microgrid

The DMPC for AC DGs has five control objectives. The first and second objectives are to guarantee the economic dispatch of the H-MG via the incremental cost consensus with AC DGs and DC DGs. The third objective is to dispatch reactive power on the AC DGs according to an economical criterion and their available capacity. The fourth and fifth objectives are to regulate the average voltage and average frequency on the AC sub-MG within secure bands to provide flexibility to the H-MG. The DMPC for AC DGs has five control objectives. The first and second objectives are to guarantee the the incremental cost consensus with DC DGs and AC DGs, thus, achieving the economic dispatch of the H-MG. The third objective is to regulate the average voltage on the DC sub-MG within secure bands to provide flexibility to the H-MG. The control scheme for the AC DG_i is depicted in Fig. 4, where the primary controller (see at the bottom) is based on frequency-active power ($\omega - P$) and voltage-reactive power ($V - Q$) droop controllers. At the DG's output, an LCL filter is placed, where the second inductance (L_i) is set set to ensure a impedance predominantly inductive [41]. The proposed DMPC for the secondary level is presented at the top. Its inputs are the local measurements/estimates ($P_i(k)$, $V_i^{ac}(k)$, $\omega_i(k)$, $\theta_i(k)$, $\hat{V}_i^{ac,B}(k)$, $\hat{\omega}_i^B(k)$, $\hat{\theta}_i^B(k)$) and the results of the optimisation problems of communicated neighbouring units. The controller has two outputs, which are the control action variations (vector $\triangle V_{s,i}^{ac}$) and the results of the local optimisation problem $\mathbb{X}_{p,i}^{ac}$ (vector of predicted values), both defined later in this section. Moreover, a complete electrical model is avoided by using the voltage measurement (V_i^{ac}) before the coupling inductance (L_i) and the voltage estimation ($\hat{V}_i^{ac,B}$) after L_i, which is computed through a non-linear reduced-order voltage observer explained in detail in [9]. Then, the phase angle difference is computed as $\delta\theta_i(k) = \theta_i(k) - \hat{\theta}_i(k)$, where $\theta_i(k)$ and $\hat{\theta}_i(k)$ are computed with PLLs.

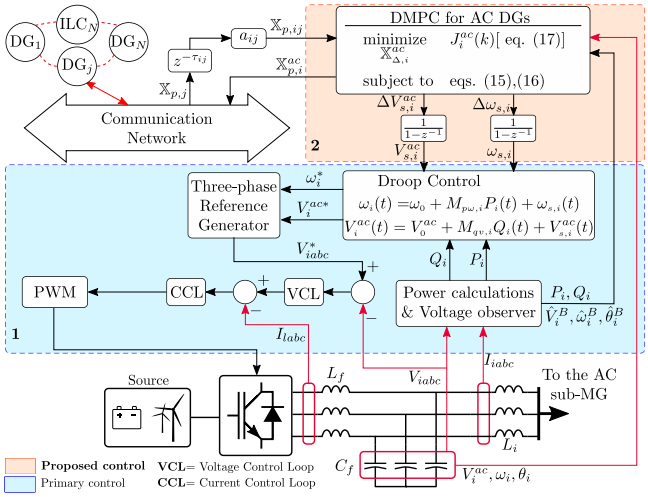

Fig. 4. Control diagram of DMPC$_i$ for AC DGs.

The linear discrete time prediction models included in the controller to rule its behaviour are detailed in (15) and (16). Model (15a) represents the incremental cost (IC) prediction model for the AC DG_i while (15b) is its reactive marginal cost (RMC) prediction model; both models were derived in Section II-B and Section II-C, respectively. Model (15c) represents the $\omega - P$ droop control. Where ω_i is the frequency, P_i^{ac} is the active power contribution, $M_{p\omega,i}$ is the droop slope, and $\triangle\omega_{s,i}$ is the frequency control action variation. Similarly, (15d) is the $V - Q$ droop control, where Q_i is the reactive power contribution, V_i^{ac} is the DG's output voltage, $M_{qv,i}$ is the droop slope, and $\triangle V_{s,i}^{ac}$ is the voltage control action variation. Model (15e) calculates the phase angle deviation ($\delta\theta_i$) throughout the inductance L_i of the LCL output filter (see at the bottom of Fig. 4). This model is used to predict the active and reactive power contributions of DG_i to the MG, where $\hat{\omega}_i^B(k)$ is the frequency estimation after L_i.

The active power contribution from AC DG_i to the MG is computed by the linearised model (15f) where $B_i = 1/(L_i \cdot \omega_0)$, ω_0 is the MG nominal frequency, $V_i^{ac}(k)$ and $\hat{V}_i^{ac,B}(k)$ are the voltage measurements and estimations before and after the inductance L_i, $P_i^{ac}(k)$ is the active power measurement, and $\delta\theta_i(k)$ is the phase angle deviation measurement. Similarly, the reactive power contribution from AC DG_i to the MG is determined by the linearized model (15g), where $Q_i(k)$ is the reactive power measurement. The active and reactive power contributions are bounded within the DG's power rating

($S_{i,max}$) through the linearised triangular constraint in (15h).

$$\eta_i^{ac}(k+m)=2a_i\ P_i^{ac}(k+m)\ +\ b_i \tag{15a}$$

$$\Psi_i(k+m)=2a_i'(k)S_{i,res}(k)Q_i(k+m)\ +\ b_i'(k) \tag{15b}$$

$$\omega_i(k+m)=\omega_i(k+m-1)+M_{p\omega,i}[P_i^{ac}(k+m)-P_i^{ac}(k+m-1)] +{}_{\triangle}\omega_{s,i}(k+m-1) \tag{15c}$$

$$V_i^{ac}(k+m)=V_i^{ac}(k+m-1)+M_{qv,i}[Q_i(k+m)-Q_i(k+m-1)] +{}_{\triangle}V_{s,i}^{ac}(k+m-1) \tag{15d}$$

$$\delta\theta_i(k+m)=\delta\theta_i(k+m-1)+T_{sec}\big[\omega_i(k+m)-\hat{\omega}_i^B(k)\big] \tag{15e}$$

$$P_i^{ac}(k+m)=P_i^{ac}(k)+[V_i^{ac}(k+m)-V_i^{ac}(k)]B_i\hat{V}_i^{ac,B}(k)\sin(\delta\theta_i(k)) +[\delta\theta_i(k+m)-\delta\theta_i(k)]B_iV_i^{ac}(k)\hat{V}_i^{ac,B}(k)\cos(\delta\theta_i(k)) \tag{15f}$$

$$Q_i(k+m)=Q_i(k)+[\delta\theta_i(k+m)-\delta\theta_i(k)]B_iV_i^{ac}(k)\hat{V}_i^{ac,B}(k)\sin(\delta\theta_i(k)) +[V_i^{ac}(k+m)-V_i^{ac}(k)]B_i\Big[2V_i^{ac}(k)-\hat{V}_i^{ac,B}(k)\cos(\delta\theta_i(k))\Big] \tag{15g}$$

$$|P_i^{ac}(k)|+|Q_i(k)|+\text{sign}(P_i^{ac}(k))[P_i^{ac}(k+m)-P_i^{ac}(k)] +\text{sign}(Q_i(k))[Q_i(k+m)-Q_i(k)]\leq S_{i,\max} \tag{15h}$$

Local approximations of the average frequency ($\overline{\omega}_i$) and the average AC voltage ($\overline{V}_i^{ac}$) are computed by models (16a) and (16b), respectively. Finally, soft constraints (16c) and (16d) work together with the cost function (see fourth and fifth terms of (17)) to maintain both average frequency and average AC voltage within predefined bands according to the recommendation of IEEE standard 1547-2018 [22] and avoid unfeasible solutions [29] by using the auxiliary variables $\omega_{aux,i}$, $V_{aux,i}^{ac}$.

$$\overline{\omega}_i(k+m)=\frac{\omega_i(k+m)+\sum\limits_{j\in\mathbb{N}_{ac}}a_{ij}(k)\omega_j(k+m-\hat{\tau}_{ij})}{1+\sum\limits_{j\in\mathbb{N}_{ac}}a_{ij}(k)} \tag{16a}$$

$$\overline{V}_i^{ac}(k+m)=\frac{V_i^{ac}(k+m)+\sum\limits_{j\in\mathbb{N}_{ac}}a_{ij}(k)V_j^{ac}(k+m-\hat{\tau}_{ij})}{1+\sum\limits_{j\in\mathbb{N}_{ac}}a_{ij}(k)} \tag{16b}$$

$$\overline{\omega}_{min}\leq\overline{\omega}_i(k+m)+\omega_{aux,i}(k+m)\leq\overline{\omega}_{max} \tag{16c}$$

$$\overline{V}_{min}^{ac}\leq\overline{V}_i^{ac}(k+m)+V_{aux,i}^{ac}(k+m)\leq\overline{V}_{max}^{ac} \tag{16d}$$

The cost function (17) comprises seven quadratic terms. The first term achieves the consensus over the ICs within the AC DGs, while the second term performs the consensus for the ICs of the DC DGs. The latter objective works only when the ILCs are enabled; the controller verifies the ILCs status (1: ON, 0:OFF) at each sample time. The third term performs the consensus over the RMC, hence guaranteeing the optimal dispatch of reactive power. The fourth and fifth terms regulate the frequency and the average AC voltage within bands by penalising the auxiliary variables $\omega_{aux,i}$ $V_{aux,i}^{ac}$. These terms temporally relax the frequency constraint (16c) and the average AC voltage constraint (16d), allowing these variables to take values outside their predefined bands for a short time. The sixth term penalises any variations of the voltage control action, and the term seventh penalises any variation of the frequency control action. Moreover, the controller achieves all the previous objectives with good transitory behaviour with only two control actions (${}_{\triangle}V_{s,i}^{ac}$ and ${}_{\triangle}\omega_{s,i}$). The terms λ_{1i} to λ_{7i} are positive tuning parameters. Note that the cooperative objectives (IC consensus with AC DGs and with DC DGs and RMC consensus) are updated only with the predicted information of communicated neighbouring DGs, represented by the terms $a_{ij}(k)$, and the estimated delays $\hat{\tau}_{ij}$.

$$\begin{aligned}J_i^{ac}(k)=&\sum_{j\in\mathbb{N}_{ac}}\sum_{m=1}^{N_y}\lambda_{1i}a_{ij}(k)\left(\eta_i^{ac}(k+m)-\eta_j^{ac}(k+m-\hat{\tau}_{ij})\right)^2\\&+\sum_{j\in\mathbb{N}_{dc}}\sum_{m=1}^{N_y}\lambda_{2i}a_{ij}(k)\left(\eta_i^{ac}(k+m)-\eta_j^{dc}(k+m-\hat{\tau}_{ij})\right)^2\\&+\sum_{j\in\mathbb{N}_{ac}}\sum_{m=1}^{N_y}\lambda_{3i}a_{ij}(k)\left(\Psi_i(k+m)-\Psi_j(k+m-\hat{\tau}_{ij})\right)^2\\&+\sum_{m=1}^{N_y}\left[\lambda_{4i}(\omega_{aux,i}(k+m))^2+\lambda_{5i}(V_{aux,i}^{ac}(k+m))^2\right]\\&+\sum_{m=1}^{N_u}\left[\lambda_{6i}({}_{\triangle}V_{s,i}^{ac}(k+m-1))^2+\lambda_{7i}({}_{\triangle}\omega_{s,i}(k+m-1))^2\right]\end{aligned} \tag{17}$$

The proposed DMPC is synthesised in a QP formulation. The optimisation vector of the QP problem comprises the predicted variables $\mathbb{X}_{p,i}^{ac}$ and the control decisions $\mathbb{X}_{\Delta,i}^{ac}$ presented in (18) and (19), respectively. The former is sent to the communication network and the first control decisions of the latter, ${}_{\triangle}V_{s,i}^{ac}(k)$, and ${}_{\triangle}\omega_{s,i}(k)$, are applied to DG_i, after passing through discrete integrators (see Fig. 4). At each sample time the optimisation problem is computed with updated measures (rolling horizon) [29].

$$\begin{aligned}\mathbb{X}_{p,i}^{ac}=[&\eta_i^{ac}(k+m),\omega_i(k+m),\delta\theta_i(k+m),V_i^{ac}(k+m),\\&\omega_{aux,i}(k+m),V_{aux,i}^{ac}(k+m),P_i^{ac}(k+m),\Psi_i(k+m),\\&Q_i(k+m),\overline{\omega}_i(k+m),\overline{V}_i^{ac}(k+m)]_{m=1}^{N_y}\end{aligned} \tag{18}$$

$$\mathbb{X}_{\Delta,i}^{ac}=[{}_{\triangle}V_{s,i}^{ac}(k+m-1),{}_{\triangle}\omega_{s,i}(k+m-1)]_{m=1}^{N_u} \tag{19}$$

In summary, all the proposed DMPCs have quadratic cost functions with linear constraints; thus, their respective minimums can be reached [26], [29]. Note that in models (12b), (15b) and (15e) to (15h) all the variables at time instant k are local measurements and estimations produced in the discretisation and linearisation of the continuous time models; they are not predicted variables. Hence, all the previous models are linear. The distributed structure allows tackling inherently communication issues and plug-and-play scenarios. Moreover,

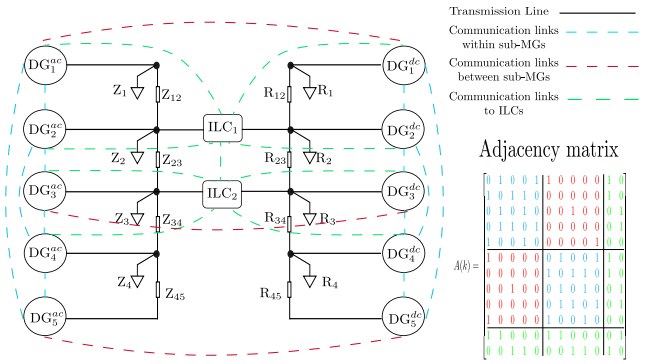

Fig. 5. H-MG topology for the validation of the DMPC scheme

TABLE II
MG PARAMETERS AND LOADS

Parameter	Description	Value
T_{prim}	Primary level sample time [s]	$1/(16 \cdot 10^3)$
L_i	DG_i^{ac} coupling inductance $[mH]$	2.5
Z_{ij}	AC sub-MG distribution lines [Ω]	$0.7 + j2.5 \cdot 2\pi$
R_i	DG_i^{dc} coupling resistor [Ω]	0.67
R_{ij}	DC sub-MG distribution lines [Ω]	0.78
$Z_1; Z_2$	AC sub-MG loads $[kVA]$	5.7+j2.3; 1.5+j0.2
$Z_3; Z_4$	AC sub-MG loads $[kVA]$	2+j0.5; 2.3+j0.3
$R_1; R_2; R_3; R_4$	DC sub-MG loads $[kW]$	3.36; 1.32; 1.13; 1.11
$P_{1,max}^{ILC}; P_{2,max}^{ILC}$	ILC: $P_{i,max}^{ILC}$	5.0; 3.0
ω_0	AC sub-MG nominal frequency	$2\pi \cdot 50$
V_0^{ac}	AC sub-MG nominal voltage	220
V_0^{dc}	DC sub-MG nominal voltage	400

each DG performs its optimisation locally; thus, the computational burden is reduced and does not increase when more DGs or ILCs are added to the H-MG. The controllers identify when the ILCs are enabled before performing the optimal dispatch in the entire H-MG. In contrast, when there are no ILCs available, the sub-MGs work independently, i.e. the optimal dispatch is performed in each sub-MG, and their voltage and frequency (on the AC sub-MG) are regulated within bands. Finally, the auxiliary variables for AC DGs and DC DGs are penalised in their respective cost functions, relaxing temporally the average frequency and average voltages inequality constraints and enabling these variables to take values outside their predefined bands for a brief time. Therefore, The optimisation problem is relaxed by using these constraints, and a feasible solution is guaranteed [26], [29], provided that the requested power is within the H-MG's physical limits.

IV. MICROGRID SETUP AND SIMULATION RESULTS

To evaluate the performance of the proposed DMPC scheme, the H-MG in Fig. 5 with electrical parameters described in Table II was simulated. It comprises an AC sub-MG with 5 AC DGs, a DC sub-MG with 5 DC DGs and two interlinking converters (ILCs). The AC distribution lines are inductive-resistive (RL), while the DC distribution lines are resistive (R). There are four LR loads on the AC sub-MG and four R loads on the DC sub-MG. The ILCs' maximum power ratings are given in Table II while the cost and operating parameters of the AC DGs and DC DGs are given in Table III. Note that in Fig. 5 the coloured dashed lines represent the communication network, and its associated adjacency matrix $\boldsymbol{A}$ is also shown at its bottom.

The MG electrical model was built in PLECS blockset®, and the primary and secondary controllers were implemented in Matlab/Simulink® environment. The primary level consists of the droop, inner voltage and current controllers. The inner voltage and current controllers were implemented as self-

TABLE III
DGS PARAMETERS

DC DGs parameters					
Parameter	DG_1^{dc}	DG_2^{dc}	DG_3^{dc}	DG_4^{dc}	DG_5^{dc}
a [$\$/kWh^2$]	0.35	0.37	0.46	0.51	0.52
b [$\$/kWh$]	1.8	2.9	2.0	2.6	1.6
Power capacity ($P_{i,max}$) [kW]	2.5				
$P-V$ droop coefficient (M_{pv}) [$\frac{V}{W}$]	$-1.2 \cdot 10^{-2}$				
AC DGs parameters					
Parameter	DG_1^{ac}	DG_2^{ac}	DG_3^{ac}	DG_4^{ac}	DG_5^{ac}
a [$\$/kWh^2$]	0.39	0.44	0.49	0.55	0.66
b [$\$/kWh$]	2.9	2.3	2.4	1.5	1.9
Power capacity ($S_{i,max}$) [kVA]	3				
$P-\omega$ droop coefficient ($M_{p\omega}$) [$\frac{rad}{sW}$]	$-3.33 \cdot 10^{-4}$				
$Q-V$ droop coefficient (M_{qv}) [$\frac{V}{VAR}$]	$-1.5 \cdot 10^{-2}$				

TABLE IV
DMPC PARAMETERS AND WEIGHTS

Parameter	**Description**	**Value**
T_{sec} [s]	Controller sample time	0.05
$\hat{\tau}_{ij}$ [s]	Estimated communication delay	0.05
Ny	Prediction horizon	10
Nu	Control horizon	10
DMPC for ILC weights		
λ_{1h} $[(kWh/\$)^2]$	Active power dispatch for DGs	$4 \cdot 10^0$
λ_{2h} [-]	Active power consensus for ILCs	$4 \cdot 10^4$
λ_{3h} $[(1/kW)^2]$	ILC control action (ΔP_h^{ILC})	$5 \cdot 10^3$
DMPC for DC DGs parameters and weights		
$[V_{max}; Vmin]$	Average voltage predefined band	[395,405]
λ_{1i} $[(kWh/\$)^2]$	Active power dispatch with DC DGs	$3.5 \cdot 10^{-4}$
λ_{2i} $[(kWh/\$)^2]$	Active power dispatch with AC DGs	$3.5 \cdot 10^{-4}$
λ_{3i} $[(1/V)^2]$	Average voltage regulation	$7 \cdot 10^3$
λ_{4i} $[(\frac{1}{V})^2]$	Voltage control action variation	$16 \cdot 10^2$
DMPC for AC DGs parameters and weights		
$[V_{max}; Vmin]$	Average voltage predefined band	[215,225]
$[\omega_{max}, \omega_{min}]$ $[rad/s]$	Frequency predefined band	$[101\pi, 99\pi]$
λ_{1i} $[(kWh/\$)^2]$	Active power dispatch with AC DGs	$2.1 \cdot 10^{-3}$
λ_{2i} $[(kWh/\$)^2]$	Active power dispatch with DC DGs	$2.1 \cdot 10^{-3}$
λ_{3i} $[(kVAR/\$)^2]$	Reactive power dispatch	$4.2 \cdot 10^1$
λ_{4i} $[(\frac{s}{rad})^2]$	Average frequency regulation	$3.8 \cdot 10^6$
λ_{5i} $[(1/V)^2]$	Average voltage regulation	$5.0 \cdot 10^5$
λ_{6i} $[(\frac{s}{rad})^2]$	Frequency control action variation	$4.5 \cdot 10^6$
λ_{7i} $[(\frac{1}{V})^2]$	Voltage control action variation	$1.9 \cdot 10^4$

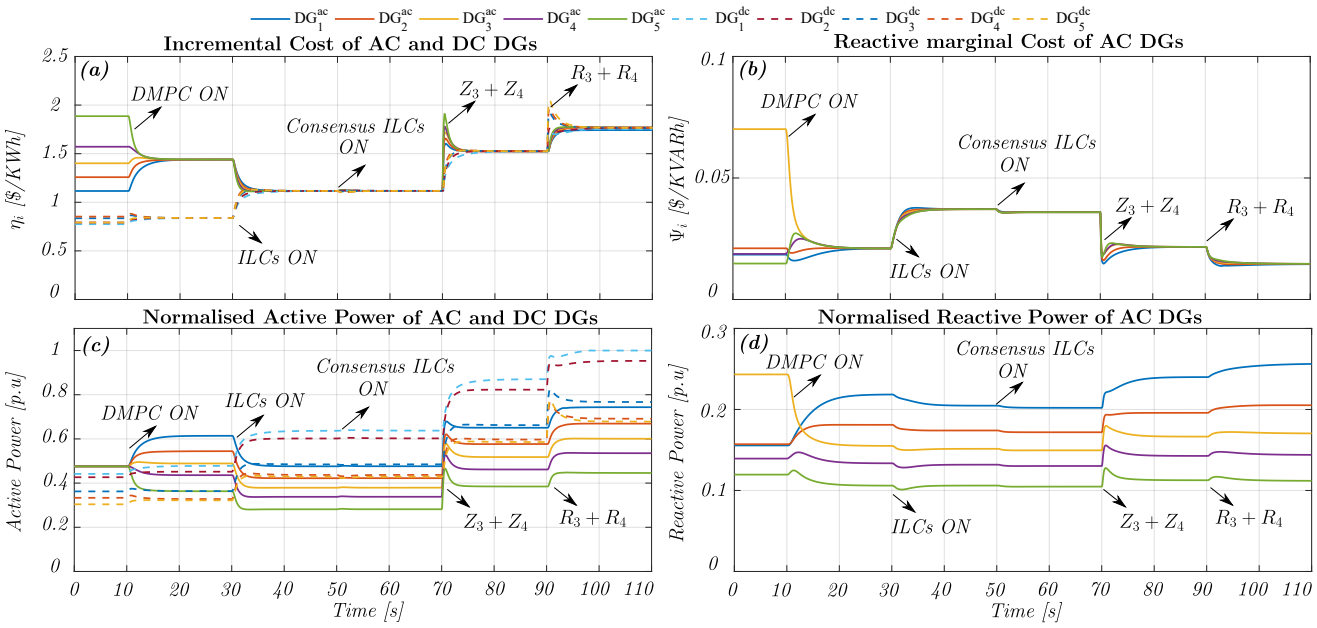

Fig. 6. Load changes: a) Incremental cost consensus, b) Reactive marginal cost consensus, c) Active power, d) Reactive power

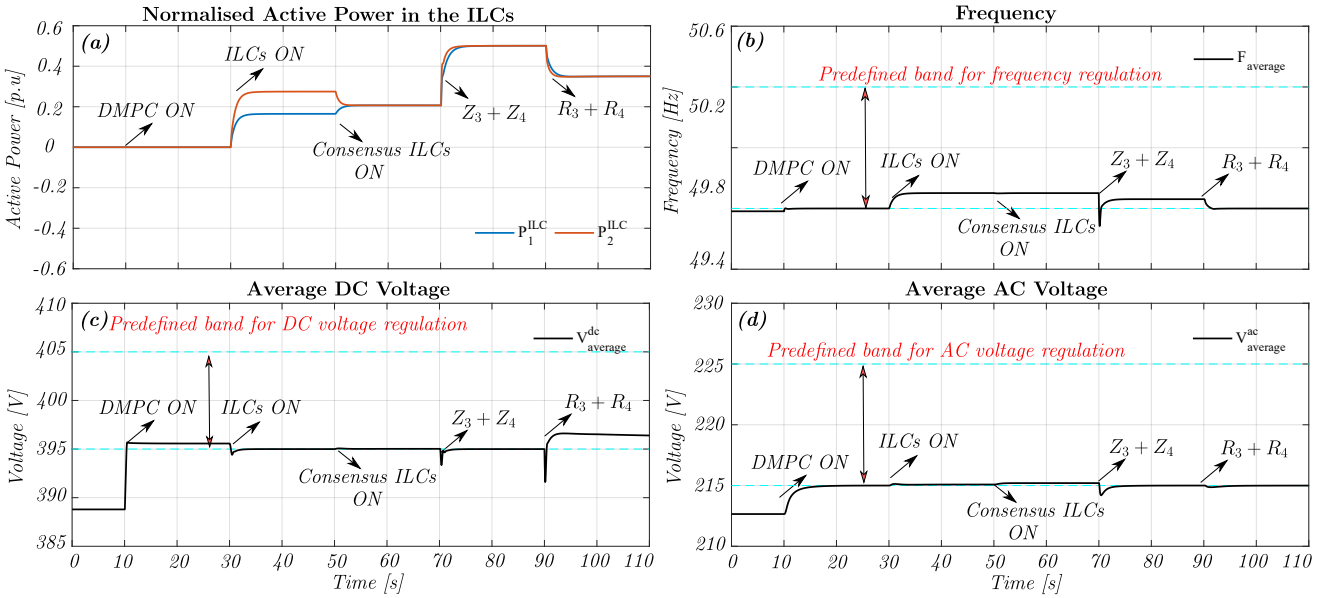

Fig. 7. Load changes: a) Active power through the ILCs, b) Frequency regulation, c) Average DC voltage regulation, d) Average AC voltage regulation. The dashed cyan lines represent the predefined band limits for the flexible variables.

tuning proportional-resonant controllers for AC variables and proportional-integral controllers for DC variables. The DMPC design parameters and weighting factors are presented in Table IV. As it is well known for predictive controllers, the computational burden is directly affected by the sample time and prediction and control horizons [29]. Therefore, these design parameters should be selected to reduce the computational burden. The sample time was chosen considering the frequency (on the AC sub-MG) and the voltage (on the DC sub-MG) open loop rise time ($T_r = 0.7s$) as $T_{sec} = 0.7/14 = 0.05s$ [42]. The prediction and control horizons were selected as ten samples to cover the transitory response of the controllers and guarantee that the controllers always find a feasible solution within the sample time [29]. Moreover, these values reduce the traffic over the communication network.

The weighting factors were tuned following the guidelines in [43], i.e., looking for a trade-off between the control objectives and, if needed giving more importance to one objective over the rest of the objectives. To fulfil the IEEE 1547-2018 standard, the average AC and DC voltages are limited to a band of ± 5 [V] of their nominal values V_0^{ac} and V_0^{dc}, respectively, while the frequency is limited to a band of $\pm\pi$ $[rad/s]$ of the nominal value ω_0. Although the limits are fixed for all the test scenarios, these can be modified as long as

they comply with IEEE standard 1547-2018 [22]. Moreover, as these limits are design parameters, they can be selected as relative or fixed values as long as they are within the IEEE 1547-2018 recommendation.

A. Scenario I (base case) - Load changes

This test evaluates the performance of the proposed DMPC scheme when the MG is subject to AC and DC load steps. For the whole test the communication network does not vary, i.e., the adjacency matrix A is kept constant and is described in Fig. 5. The test starts with both AC DGs and DC DGs enabled and working only with the primary control while the ILC is disabled. Hence, the AC sub-MG and the DC sub-MG are working separately, and its dynamic is fixed by the droop controller. Additionally Z_1, Z_2, R_1, and R_2 are connected at their respective nodes (see Fig. 5). Note that as the DMPC controllers are disabled, there are neither consensus in the incremental cost (IC) nor consensus in the reactive marginal cost (RMC) (see Fig. 6.a and Fig. 6.b before $t = 10s$); therefore, active and reactive power are not optimally dispatched (see Fig. 6.c and Fig. 6.d before $t = 10s$). Furthermore, the frequency and average AC and DC voltages of the H-MG are outside of the established bands (see Fig. 7.b, Fig. 7.c and Fig. 7.d before $t = 10s$).

At $t = 10s$, the predictive controllers for the sub-MGs are enabled, but the ILCs are still disabled, so there is no power transference between the sub-MGs yet. Therefore, the DMPC controllers optimise the DGs' performance locally, i.e., the second terms (objectives) in the cost functions of (13) and (17) are disabled. It is observed that on the AC sub-MG, consensus on both the IC and RMC are achieved (see Fig. 6.a and Fig. 6.b at $t = 10s$); thus, both active and reactive power are redispatched optimally, considering generation costs (see Fig. 6.c and Fig. 6.d at $t = 10s$). Moreover, both frequency and average AC voltage are regulated within the established bands (see Fig. 7.b and Fig. 7.d at $t = 10s$). Similarly, on the DC sub-MG, the consensus on the IC is achieved, hence active power is redispatched based on the DGs' generation costs, as shown in Fig. 6.a and Fig. 6.c at $t = 10s$. Additionally, the average DC voltage is regulated within its established band (see Fig. 7.c at $t = 10s$).

The ILCs and their DMPC strategies are enabled at $t = 30s$, but initially only the IC consensus objective (second term) in (9) is enable. Thus, the ILCs equalise the ICs on both sub MGs to achieve global economic dispatch (see Fig. 6.a at $t = 30s$), but they do not transfer active power proportionally to their power rating (see Fig. 7.a at $t = 30s$), which could cause overloading in the ILCs. Fig. 6.c shows that the DGs on the DC sub-MG increase their power contribution to transfer power to the AC sub-MG because they have lower generation costs (see Table III) while the AC DGs decrease theirs, as they are more expensive. At $t = 50s$, the power consensus on the ILCs is enabled (third term) in (9). Therefore, both ILCs transfer power proportionally to their power rating, as shown in Fig. 7.a at $t = 50s$.

Then, at $t = 70s$ the total AC load (Z_3 and Z_4) is connected. As the DC DGs are cheaper, they increase more their power contribution than the AC DGs (see Fig. 6.c at $t = 70s$) to transfer more through the ILCs (see Fig. 7.a at $t = 70s$) and achieve the optimal dispatch point (see Fig. 6.a at $t = 70s$). Furthermore, this event takes the frequency and voltages outside of their bands; however, these variables are regulated immediately by the DMPC controllers, as shown in Fig. 7.b, Fig. 7.c, and Fig. 7.d at $t = 70s$. Finally, at $t = 90s$, R_3 and R_4 are connected; hence, the H-MG is subject to its total load. Due to the DC sub-MG increasing their load consumption and the DC DGs being cheaper, this new load is mostly supplied by its local DGs. Moreover, as two DC DGs almost reach their power rating limit, the AC DGs also increase their power contribution to supply the remaining load. Therefore, the power transferred through the ILCs is reduced. It is observed that the optimal dispatch of active and reactive power is fulfilled under this demanding operating condition. Moreover, despite the sudden perturbations, the frequency and voltages are regulated within their bands all the time. The results show that the proposed DMPC scheme achieves all the objectives without large overshoots and settling times below 8 seconds during all the events. Furthermore, All the constraints are respected.

B. Scenario II - Comparison against a DAPI-based strategy without economic dispatch

This section presents a comparison study between the proposed DMPC strategy and the reported technique in [3]. The DAPI-based method in [3] shares active and reactive power proportionally to the DGs' power rating without considering the DGs generation costs and restores frequency and voltage to nominal values. The same simulator and adjacency matrix (A) presented in Fig. 5 is used for this comparison study. The selected scenario is communication delays, one of the most common phenomena in distributed controllers. A communication delay of one second is applied in the entire communication network $(\tau_{ij} = 1s)$ for the whole test. For this test, both the proposed DMPC strategy and the DAPI strategy [3] start with all their functionalities enabled and all the loads connected except R_3 and R_4. Fig. 8 presents on the left-hand side the results of active power contribution and active power transference through the ILCs for [3], while the results of these variables for the proposed DMPC are on the right-hand side. Conversely, Fig. 9 presents in each graph a performance comparison of both control strategies.

At $t = 10s$, the H-MG is subject to its total load, i.e., R_3 and R_4 are connected. It is observed that the DAPI controller shares power proportionally while the proposed DMPC dispatches the DGs considering their operation costs (see Fig. 8.a and Fig. 8.b at $t = 10s$). The proposed DMPC transfers more active power through the ILCs than the DAPI controller (see Fig. 8.c and Fig. 8.d at $t = 10s$); this is because the DMPC achieves the economical dispatch point by dispatching more power from the DC DGs, as these are cheaper (see Table III). Furthermore, when the H-MG has its total load connected, the operation cost is reduced by up to 4.55%, i.e., from 62.25 $\$/h$ to 59.42 $\$/h$, as shown in Fig. 9.a. Regarding frequency and voltage, the DAPI controller restores

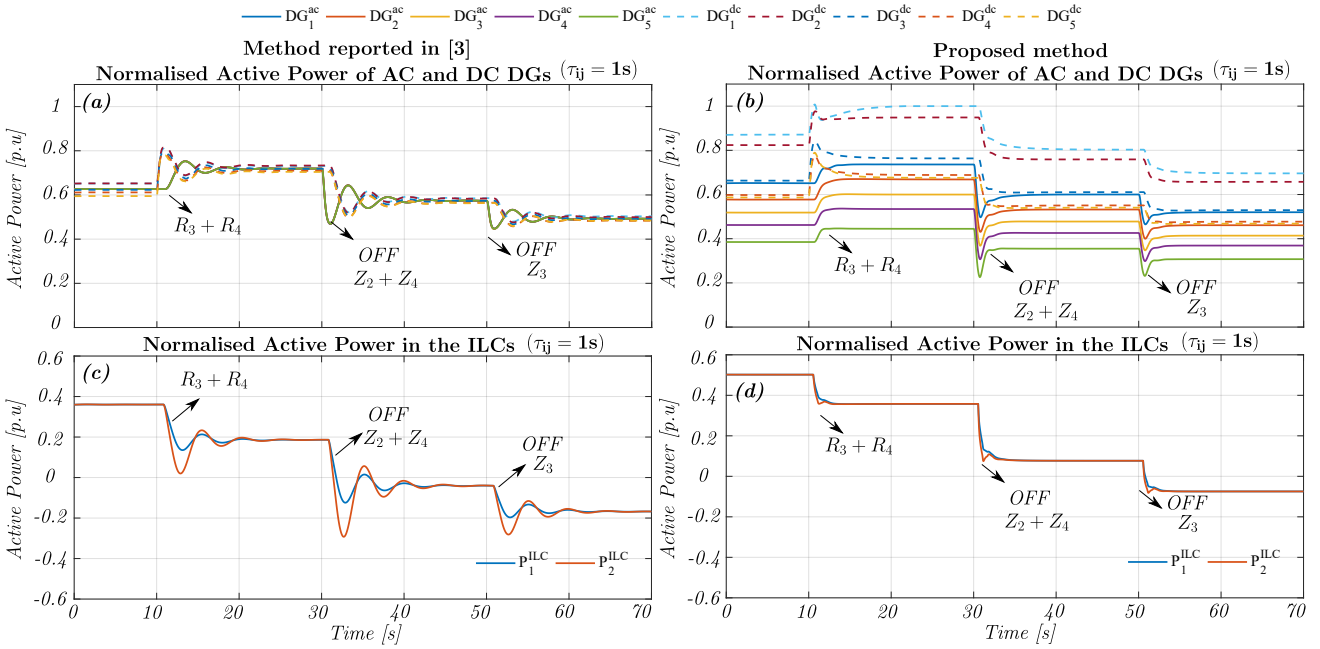

Fig. 8. Comparison between the proposed DMPC scheme and the method reported in [3]for ($\tau_{ij} = 1s$): a)-b) Active power for both methods, c)-d) Active power through the ILCs for both methods.

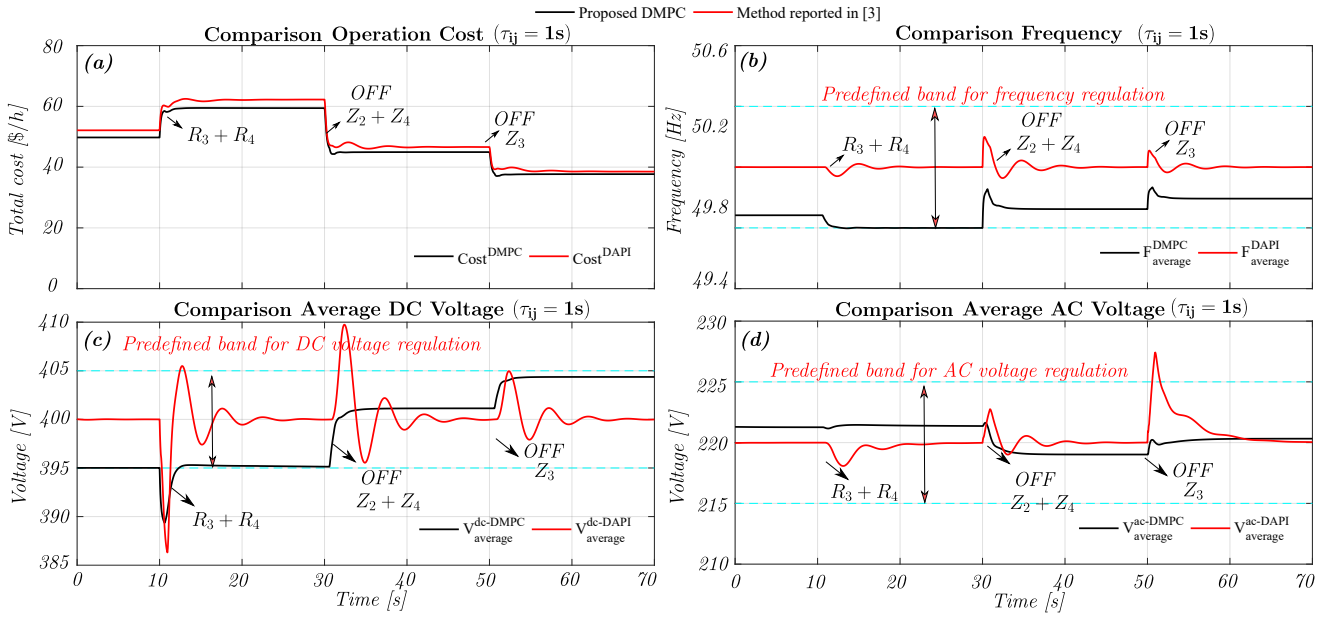

Fig. 9. Comparison between the proposed DMPC scheme and the method reported in [3] for ($\tau_{ij} = 1s$): a) Total operating cost, b) Frequency regulation, c) Average DC voltage regulation, d) Average AC voltage regulation. The dashed cyan lines represent the predefined band limits for the flexible variables.

these variables to nominal values while the proposed DMPC provides more flexibility to the H-MG and regulates them only when they are outside their established bands, as shown in Fig. 9.b, Fig. 9.c and Fig. 9.d. The results demonstrate that the proposed controller is capable of controlling the frequency and average voltages within their predefined bands, allowing temporal violations during transients. This is achieved via soft constraints and high penalisation of the predicted auxiliary variables in their respective cost functions.

It is crucial to note that the DAPI controller is highly affected by the large communication delay ($\tau_{ij} = 1s$); this controller presents larger overshoots and settling times than the DMPC in all their controlled variables. This poor performance is because the DAPI controller does not provide a delay compensation mechanism. On the other hand, the proposed DMPC controller possesses a delay estimation and the rolling horizon property, which correct the control action sequences and compensate for the effects of delays [27].

Finally, at $t = 30s$ and at $t = 50s$, Z_2 and Z_4, and Z_3 are disconnected, respectively. The results during these events

are consistent with the previously described performance. In summary, the communication delay affects the behaviour of [3] significantly by increasing its overshoots and settling time, while the proposed DMPC is slightly affected with negligible overshoots. Moreover, the proposed DMPC has a lower operation cost during the entire test. This is because the proposed DMPC uses cost-effectively the DGs of the H-MG. Despite the cost reduction of 4.55% seems minimal in monetary terms due to the small size of the H-MG, it could be significant in percentage terms in a larger H-MG. Furthermore, the DMPC scheme can simultaneously regulate variables to specific values and within bands, providing more flexibility to the H-MG while physical constraints are satisfied. Additionally, the DMPC can tackle more control objectives with fewer control actions, while in the DAPI method, a new controller needs to be designed (added) for each control objective.

V. Conclusion

This paper presented a novel DMPC strategy for isolated H-MGs to tackle simultaneously the economic dispatch of both active power and reactive power and the regulation within bands of frequency and voltages through the use of soft constraints (fulfilling IEEE standard 1547-2018). Specifically, the frequency and the average AC voltage on the AC sub-MG and the average DC voltage on the DC sub-MG are regulated within bands. The DMPC scheme considers the H-MG as a single entity by modelling the behaviour and interaction of AC DGs, DC DGs and ILCs in their cost functions.

The dynamic performance of the proposed DMPC scheme is evaluated and discussed under load impacts and communication delays scenarios. Moreover, a detailed comparison with a reported work is presented. In all the tests, the DMPC fulfils its objectives without exceeding the maximum power rating limits, preventing the overloading of DGs and ILCs. It is verified that the proposed DMPC strategy reduces the H-MG's operation costs by up to 4.55%, which in a larger H-MG represents significant savings. Moreover, the proposed DMPC scheme is robust in the presence of communication delays, providing good behaviour when significant delays occur in the whole H-MG. Future research will be focused on the extension of the proposal for adding objectives such as ILCs' power transfer losses minimisation, line losses reduction, THD constraints, grid-connected operation and imbalance sharing in H-MGs. Given that a stability analysis using non-iterative methods has not been carried out as yet, we are exploring new approaches to achieve a formal stability analysis of the proposed control scheme, which will be presented in future research.

References

[1] S. K. Sahoo, A. K. Sinha, and N. K. Kishore, "Control Techniques in AC, DC, and Hybrid AC–DC Microgrid: A Review," *IEEE J. Emerg. Sel. Top. Power Electron.*, vol. 6, no. 2, pp. 738–759, Jun. 2018.

[2] E. Rute-Luengo, A. Navas-Fonseca, J. S. Gómez, E. Espina, C. Burgos-Mellado, D. Sáez, M. Sumner, and D. Muñoz-Carpintero, "Distributed model-based predictive secondary control for hybrid ac/dc microgrids," *IEEE Trans. Emerg. Sel. Topics Power Electron.*, pp. 1–1, 2022.

[3] E. Espina, R. Cardenas-Dobson, J. W. Simpson-Porco, D. Saez, and M. Kazerani, "A Consensus-Based Secondary Control Strategy for Hybrid AC/DC Microgrids with Experimental Validation," *IEEE Trans. Power Electron.*, vol. 36, no. 5, pp. 5971–5984, May 2021.

[4] J. M. Guerrero, J. C. Vásquez, J. Matas, L. G. de Vicuna, and M. Castilla, "Hierarchical control of droop-controlled ac and dc microgrids—a general approach toward standardization," *IEEE Trans. Ind. Electron.*, vol. 58, no. 1, pp. 158–172, Jan. 2011.

[5] Y. Zheng, S. Li, and R. Tan, "Distributed model predictive control for on-connected microgrid power management," *IEEE Trans. Control Syst. Technol.*, vol. 26, no. 3, pp. 1028–1039, 2018.

[6] F. Dörfler, S. Bolognani, J. W. Simpson-Porco, and S. Grammatico, "Distributed control and optimization for autonomous power grids," in *2019 18th European Control Conference (ECC)*, 2019, pp. 2436–2453.

[7] M. Zaery, P. Wang, W. Wang, and D. Xu, "Distributed Global Economical Load Sharing for a Cluster of DC Microgrids," *IEEE Trans. Power Syst.*, vol. 35, no. 5, pp. 3410–3420, Sep. 2020.

[8] R. Babazadeh-Dizaji and M. Hamzeh, "Distributed Hierarchical Control for Optimal Power Dispatch in Multiple DC Microgrids," *IEEE Syst. J.*, vol. 14, no. 1, pp. 1015–1023, Mar. 2020.

[9] A. Navas-Fonseca, J. S. Gomez, J. Llanos, E. Rute, D. Saez, and M. Sumner, "Distributed Predictive Control Strategy for Frequency Restoration of Microgrids Considering Optimal Dispatch," *IEEE Trans. Smart Grid*, vol. 12, no. 4, pp. 2748–2759, Jul. 2021.

[10] J. Llanos, D. E. Olivares, J. W. Simpson-Porco, M. Kazerani, and D. Saez, "A novel distributed control strategy for optimal dispatch of isolated microgrids considering congestion," *IEEE Trans. Smart Grid*, vol. 10, no. 6, pp. 6595–6606, Nov. 2019.

[11] G. Chen and Z. Guo, "Distributed secondary and optimal active power sharing control for islanded microgrids with communication delays," *IEEE Trans. Smart Grid*, vol. 10, no. 2, pp. 2002–2014, Mar. 2017.

[12] Z. Yi, Y. Xu, W. Gu, and Z. Fei, "Distributed model predictive control based secondary frequency regulation for a microgrid with massive distributed resources," *IEEE Trans. Sustain. Energy*, vol. 12, no. 2, pp. 1078–1089, 2021.

[13] B. Abdolmaleki and Q. Shafiee, "Online kron reduction for economical frequency control of microgrids," *IEEE Trans. Ind. Electron.*, vol. 67, no. 10, pp. 8461–8471, 2020.

[14] Z. Li, Z. Cheng, J. Si, and S. Li, "Distributed event-triggered hierarchical control to improve economic operation of hybrid ac/dc microgrids," *IEEE Trans. Power Syst*, pp. 1–1, 2021.

[15] W. Feng, J. Yang, Z. Liu, H. Wang, M. Su, and X. Zhang, "A unified distributed control scheme on cost optimization for hybrid ac/dc microgrid," in *2018 IEEE 4th South. Power Electron. Conf. (SPEC)*, Dec. 2018, pp. 1–6.

[16] A. Navas-Fonseca, C. Burgos-Mellado, J. S. Gómez, F. Donoso, L. Tarisciotti, D. Sáez, R. Cárdenas, and M. Sumner, "Distributed predictive secondary control for imbalance sharing in ac microgrids," *IEEE Trans. Smart Grid*, vol. 13, no. 1, pp. 20–37, 2022.

[17] X. Zhao, L. Meng, T. Dragicevic, M. Savaghebi, J. M. Guerrero, J. C. Vasquez, and X. Wu, "Distributed low voltage ride-through operation of power converters in grid-connected microgrids under voltage sags," in *IECON 2015 - 41st Annual Conference of the IEEE Industrial Electronics Society*, 2015, pp. 001 909–001 914.

[18] Y. Khayat, Q. Shafiee, R. Heydari, M. Naderi, T. Dragičević, J. W. Simpson-Porco, F. Dörfler, M. Fathi, F. Blaabjerg, J. M. Guerrero, and H. Bevrani, "On the secondary control architectures of ac microgrids: An overview," *IEEE Trans. Power Electron.*, vol. 35, no. 6, pp. 6482–6500, Jun. 2020.

[19] D. K. Molzahn, F. Dörfler, H. Sandberg, S. H. Low, S. Chakrabarti, R. Baldick, and J. Lavaei, "A survey of distributed optimization and control algorithms for electric power systems," *IEEE Trans. Smart Grid*, vol. 8, no. 6, pp. 2941–2962, 2017.

[20] F. L. Lewis, H. Zhang, K. Hengster-Movric, and A. Das, *Cooperative Control of Multi-Agent Systems*, ser. Communications and Control Engineering. London: Springer London, 2014.

[21] L. Ding, Q.-L. Han, and X.-M. Zhang, "Distributed secondary control for active power sharing and frequency regulation in islanded microgrids using an event-triggered communication mechanism," *IEEE Trans. Industr. Inform.*, vol. 15, no. 7, pp. 3910–3922, 2019.

[22] IEEE Standard Association, *IEEE Std. 1547-2018. Standard for interconnection and interoperability of distributed energy resources with associated electric power systems interfaces*. IEEE, 2018.

[23] G. Van den Broeck, J. Stuyts, and J. Driesen, "A critical review of power quality standards and definitions applied to dc microgrids," *Applied Energy*, vol. 229, pp. 281–288, 2018. [Online]. Available: https://www.sciencedirect.com/science/article/pii/S0306261918310869

[24] I. S. Association, "Ieee recommended practice for 1 kv to 35 kv medium-voltage dc power systems on ships," *IEEE Std 1709-2018 (Revision of IEEE Std 1709-2010)*, pp. 1–54, 2018.

[25] A. Navas-Fonseca, C. Burgos-Mellado, J. S. Gómez, J. Llanos, E. Espina, D. Sáez, and M. Sumner, "Distributed predictive control using frequency and voltage soft constraints in ac microgrids including economic dispatch of generation," in *IECON 2021 – 47th Annual Conference of the IEEE Industrial Electronics Society*, 2021, pp. 1–7.

[26] C. Bordons, F. Garcia-Torres, and M. A. Ridao, *Model predictive control of microgrids*, 1st ed., ser. Advances in Industrial Control. Springer International Publishing, 2020.

[27] J. Hu, Y. Shan, J. M. Guerrero, A. Ioinovici, K. W. Chan, and J. Rodriguez, "Model predictive control of microgrids – an overview," *Renew. Sust. Energ. Rev.*, vol. 136, p. 110422, Feb. 2021.

[28] O. Babayomi, Z. Zhang, T. Dragicevic, R. Heydari, Y. Li, C. Garcia, J. Rodriguez, and R. Kennel, "Advances and opportunities in the model predictive control of microgrids: Part II–Secondary and tertiary layers," *Int. J. Electr. Power Energy Syst.*, vol. 134, p. 107339, Jan. 2022.

[29] E. F. Camacho and C. Bordons, "Constrained model predictive control," in *Model Predictive Control*, 2nd ed., ser. Advanced Textbooks in Control and Signal Processing. London: Springer London, 2007.

[30] P. C. Loh, D. Li, Y. K. Chai, and F. Blaabjerg, "Autonomous operation of hybrid microgrid with ac and dc subgrids," *IEEE Trans. Power Electron.*, vol. 28, no. 5, pp. 2214–2223, May 2013.

[31] H. J. Yoo, T. T. Nguyen, and H. M. Kim, "Consensus-based distributed coordination control of hybrid AC/DC microgrids," *IEEE Trans. Sustain. Energy*, vol. 11, no. 2, pp. 629–639, Apr. 2020.

[32] J. Zhou, H. Zhang, Q. Sun, D. Ma, and B. Huang, "Event-based distributed active power sharing control for interconnected ac and dc microgrids," *IEEE Trans. Smart Grid*, vol. 9, no. 6, pp. 6815–6828, Nov. 2018.

[33] J.-W. Chang, G.-S. Lee, S.-I. Moon, and P.-I. Hwang, "A novel distributed control method for interlinking converters in an islanded hybrid ac/dc microgrid," *IEEE Trans. Smart Grid*, vol. 12, no. 5, pp. 3765–3779, Sep. 2021.

[34] Y. Zhao, M. Irving, and Y. Song, "A cost allocation and pricing method for reactive power service in the new deregulated electricity market environment," in *2005 IEEE/PES Transmission Distribution Conference Exposition: Asia and Pacific*, 2005, pp. 1–6.

[35] S. M. Sadek, W. A. Omran, M. A. M. Hassan, and H. E. A. Talaat, "Data driven stochastic energy management for isolated microgrids based on generative adversarial networks considering reactive power capabilities of distributed energy resources and reactive power costs," *IEEE Access*, vol. 9, pp. 5397–5411, 2021.

[36] I. Serban, S. Céspedes, C. Marinescu, C. A. Azurdia-Meza, J. S. Gómez, and D. S. Hueichapan, "Communication requirements in microgrids: A practical survey," *IEEE Access*, vol. 8, pp. 47 694–47 712, 2020.

[37] A. S. Soliman, A. A. Saad, and O. Mohammed, "Securing networked microgrids with dnp3 protocol," in *2021 IEEE International Conference on Environment and Electrical Engineering and 2021 IEEE Industrial and Commercial Power Systems Europe (EEEIC / I&CPS Europe)*, 2021, pp. 1–6.

[38] B. Yoo, H.-S. Yang, S. Yang, Y.-s. Jeong, and W.-y. Kim, "Can to iec 61850 for microgrid system," in *2011 International Conference on Advanced Power System Automation and Protection*, vol. 2, 2011, pp. 1219–1224.

[39] Y. jun Zhang and Z. Ren, "Optimal reactive power dispatch considering costs of adjusting the control devices," *IEEE Trans. Power Syst*, vol. 20, no. 3, pp. 1349–1356, Aug. 2005.

[40] J. S. Gomez, D. Saez, J. W. Simpson-Porco, and R. Cardenas, "Distributed predictive control for frequency and voltage regulation in microgrids," *IEEE Trans. Smart Grid*, vol. 11, no. 2, pp. 1319–1329, Mar. 2020.

[41] M. Ben Said-Romdhane, M. W. Naouar, I. S. Belkhodja, and E. Monmasson, "An Improved LCL Filter Design in Order to Ensure Stability without Damping and Despite Large Grid Impedance Variations," *Energies 2017, Vol. 10, Page 336*, vol. 10, no. 3, p. 336, Mar. 2017.

[42] K. J. Åström and B. Wittenmark, *Adaptive Control*. Addison-Wesley, 1989.

[43] J. Rossiter, *Model-Based Predictive Control: A Practical Approach (Control Series)*, 1st ed. CRC Press, 2017.

Alex Navas-Fonseca (Student Member, IEEE) received the B.Sc. degree in electronics engineering (Hons.) from Universidad de las Fuerzas Armadas-ESPE, Ecuador in 2015, and the PhD degrees in Electrical and Electronics Engineering from The University of Nottingham, U.K., and The University of Chile in 2022. Currently, he is a lecturer at the Department of Engineering Sciences at Universidad Andrés Bello, Chile and a researcher at the Energy Transformation Center at the same university. His research interests include the control and management of microgrids, distributed model predictive control applied to microgrids and renewable energies, cyber-attack issues in microgrids, and demand side management techniques.

Claudio Burgos-Mellado (Member, IEEE) was born in Cunco, Chile. He received the B.Sc. and M.Sc. degrees in electrical engineering from the University of Chile, Santiago, Chile, in 2012 and 2013, respectively, and the dual Ph.D. degree in electrical and electronic engineering from the University of Nottingham, U.K., and in electrical engineering from the University of Chile, Santiago, Chile in 2019. From 2019 to 2021, he was a Research Fellow in the Power Electronics, Machines and Control Group (PEMC group) at the University of Nottingham, United Kingdom. Currently, he is an Assistant Professor with the Institute of Engineering Sciences, Universidad de O'Higgins, Rancagua, Chile. His current interests include battery energy storage systems, electrical vehicle technologies, power electronics, microgrids, power quality issues, modular multilevel converters, and cybersecurity issues on electrical systems. In 2021, he received the best PhD thesis award in the category of Exact Science from the Chilean Academy of Sciences.

Juan S. Gómez received his degree in Electronics Engineering from "Universidad Distrital- Francisco José de Caldas", Bogotá-Colombia in 2011, and the Ph.D. degree in Electrical Engineering from the University of Chile (Universidad de Chile), Santiago-Chile in 2020. Currently, he is afiliated as assistant professor at the Engineering Faculty and the Energy transformation Center of Universidad Andrés Bello, Santiago-Chile. He performed as postdoctoral researcher on microgrids applications for mining industry at the Pontificia Universidad Católica de Chile. His research interests are focused mainly on power quality, ancillary services in power systems, networked control systems, renewable energies, model-based predictive control, and microgrids control.

Enrique Espina was born in Santiago, Chile. In 2013, he received the B.Sc. degree in electrical engineering from the University of Santiago of Chile, Santiago, Chile. In 2017, he received the M.Sc. degree in electrical engineering from the University of Chile, Santiago, Chile, and the dual Ph.D. degrees from the University of Chile, Santiago, Chile, and the University of Waterloo, Waterloo, Ontario, Canada, in 2021. He is an Assistant Professor with the Department of Electrical Engineering, University of Santiago of Chile, Santiago, Chile. His research interests include the control and operation of hybrid ac/dc microgrids, energy storage systems, electrical vehicle technologies, renewable energies and power electronic converters.

Jacqueline Llanos (Member, IEEE) was born in Latacunga, Ecuador. She received the B.Sc. and Engineer degrees in electronic engineering from the Army Polytechnic School, Ecuador. She received the M.Sc. and Ph.D. degrees in electrical engineering from the University of Chile, Santiago. She is currently an Assistant Professor with the Department of Electrical and Electronic, Universidad de las Fuerzas Armadas ESPE, Ecuador. Her current research interests include control and management of microgrids, control of power generation plants, distributed control and predictive control.

Doris Sáez (Senior Member, IEEE) was born in Panguipulli, Chile. She received the M.Sc. and Ph.D. degrees in electrical engineering from the Pontificia Universidad Católica de Chile, Santiago, Chile, in 1995 and 2000, respectively. She is currently a Full Professor with the Department of Electrical Engineering and the Head of the Indigenous People Program, Faculty of Mathematical and Physical Sciences, University of Chile, Santiago. She has coauthored the books Hybrid Predictive Control for Dynamic Transport Problems (Springer Verlag, 2013) and Optimization of Industrial Processes at Supervisory Level: Application to Control of Thermal Power Plants (Springer-Verlag, 2002). Her research interests include predictive control, fuzzy control design, fuzzy identification, and control of microgrids. She also serves as an Associate Editor for the IEEE Transactions on Smart Grid.

Mark Sumner (Senior Member, IEEE) received the B.Eng degree in Electrical and Electronic Engineering from Leeds University in 1986 and then worked for Rolls Royce Ltd in Ansty, UK. Moving to the University of Nottingham, he completed his PhD in induction motor drives in 1990, and after working as a research assistant, was appointed Lecturer in October 1992. He is now Professor of Electrical Energy Systems. His research interests cover control of power electronic systems including power electronics for enhanced power quality, stability of power electronic convertors and novel power system fault location strategies.

Daniel E. Olivares (Member, IEEE) was born in Santiago, Chile. He received the B.Sc. and Engineering degrees in electrical engineering from the University of Chile, Santiago, in 2006 and 2008, respectively, and the Ph.D. degree in electrical and computer engineering from the University of Waterloo, Waterloo, ON, Canada, in 2014. He is currently an Associate Professor in the Faculty of Engineering and Sciences, and Director of the Center for Energy Transition, at Adolfo Ibañez University, Chile, Adjunct Associate Professor of the Electrical & Computer Engineering Department at the University of Waterloo, and is Associate Reseacher of the Institute Complex Engineering Systems (ISCI). His research interests include modeling, simulation, and control, and optimization of power systems in the context of smart grids.